IMPACT PRESSURE ESTIMATION OF AN AVALANCHE ON A STRUCTURE AS DEDUCED FROM INVERSE ANALYSIS AND MONTE CARLO SENSITIVITY SIMULATIONS

D. Baroudi[1], E. Thibert[2*], X. Ravanat[2], A. Limam[1]
[1] LGCIE, INSA, 20 Av. Albert Einstein, 69621 Villeurbanne, France
[2] ETNA, Cemagref, 2 rue de la Papeterie, 38402 Saint Martin d'Hères Cedex

ABSTRACT. Avalanche impact pressure on a flat surface structure has been quantified by full scale experiments performed at the Lautaret avalanche test site (France). An inverse analysis method is developed to reconstruct the pressure applied on this macroscopic sensor from the deformations recorded during the impact. The deformation-to-pressure transfer function of the sensor is determined by analytical modelling and in-situ impact hammer tests. The transfer function is used to quantify the pressure of a 17 m/s avalanche artificially released on the structure. In order to access to the uncertainty of the reconstructed pressure, an advanced sensibility analysis is performed. Firstly, the uncertainties related to different parameters and processes involved are identified and estimated in the deformation-to-pressure transfer function through probability distributions. Then, the sensibility of the reconstructed pressure to these parameters is investigated to identify the most contributing parameters. Finally, the distribution of the uncertainty is estimated as a probability density of the total error/uncertainty in the pressure via a Monte Carlo simulation.

KEYWORDS: Avalanche, impact pressure, inverse analysis, error analysis, Monte Carlo simulations.

1. INTRODUCTION

Designing passive avalanche defense structures and zoning avalanche hazard are limited by our poor knowledge of the action of a snow avalanche against an obstacle. As no constitutive equation is available for flowing snow, flow-structure interactions remain therefore largely investigated by experimental studies. Among them, full-scale experiments are mainly important in that they validate small-scale experiments or numerical models and provide phenomenological information (Sovilla et al., 2008; Berthet-Rambaud et al., 2008; Thibert et al. 2008). Most of full-scale studies dedicated to the estimation of pressure in avalanche have used small load cells to obtain insight into the avalanche structure and pressure distribution (Lang and Brown, 1980; Schaerer and Salway, 1980; McClung and Schaerer, 1985; Norem et al., 1985; Kawada et al., 1989; Nishimura et al. 1989, Abe et al., 1991; Schaer and Issler 2001; Sovilla et al., 2008).

* *corresponding author address:* Dr. E. Thibert, ETNA (Cemagref), BP76, 2 rue de la papeterie, 38402 Saint Martin d'Hères Cedex., emmanuel.thibert@cemagref.fr.

Because such measurements are highly intrusive, a different approach has been proposed (Berthet-Rambaud et al., 2008; Thibert et al. 2008): A suitable experimental structure is set up in a real path, and the pressure is to be determined from an inverse analysis of the deformation of the structure measured during the avalanche. The low Eigen frequencies of the sensor-structure force to conduct a spectral analysis of the structure to acquire the deformation to pressure frequency transfer function.

This approach provides measurements at a scale where the avalanche can be modelled by fluid mechanics equations. It has shown its potential to provide basic understandings of flow-structure interaction processes (Thibert et al., 2008). Here, we extend the analysis and the data process with an error analysis based on Monte Carlo simulations.

2. METHOD

2.1 Study Site and experimental set up

Experiments are carried out at the Lautaret full-scale avalanche test site in the southern French Alps (45.033°N/6.404°E). This

site has been extensively described in previous papers (Issler, 1999; Berthet-Rambaud et al., 2008; Thibert et al. 2008), so that only a short description is given here.

The avalanche path n°2 is used for this experiment (Fig. 1). Its length is 500 m with an average slope angle of 36° that reaches 40° in the starting zone. The instrumented structure is a one square-meter plate supported by a 3.5 m high steel cantilever, facing the avalanche, and fixed in a strong concrete foundation (Fig. 2). The plate can be moved along the beam to be located exactly at the surface of the initial snow-cover prior to avalanche release. It represents a large obstacle in comparison to the flow height and therefore integrates the effects of flow heterogeneities. Strains are measured at the bottom of the beam with precision strain gages placed in the maximum bending moment area. Sampling rate for data acquisition is set at 3000 Hz to record dynamic effects. Signals are filtered with a cut-off frequency of 1000 Hz to ensure a bandwidth without aliasing.

2.2 Inverse analysis

The inverse analysis procedure is developed using dynamic strain measurements performed at the bottom of the structure. The avalanche action is assumed to be uniformly distributed over the plate. No avalanche force is assumed to act directly on the beam which is designed to remain elastic during avalanche loading, perfectly clamped at one end and free elsewhere. The equations of motion are those of structural dynamics (Gerardin and Rixen, 1993) and an Euler-Bernoulli beam model is used.

Figure 1: Avalanche artificially released on the 15 February 2007 in path n°2 where the instrumented structure is set up.

The direct problem consists in evaluating the strain history from the loading, boundary and initial conditions. Using the Euler-Bernoulli beam model, the direct problem is firstly solved by assuming that the impacting force acts at a specific point. As described by Meirovitch (1986), this formulation is equivalent to solving a Fredholm integral equation of the first order:

$$\varepsilon_i(t) = \sum_j \int_0^t h_{ij}(t-\tau) f_j(\tau) d\tau \qquad (1)$$

where ε_i is the strain history measured at a point x_i (gage locations), f_j the impact load at x_j (center of the plate) and h_{ij} the transfer function between excitation and measurement points. The transfer function or its equivalent Frequency Response Function (FRF) in the frequency domain (ω: angular frequency), $\hat{h}(\omega)$, is known once the mechanical model of the structure including its boundary conditions has been set (Fig. 3). The FRFs can be also directly measured from impact hammer tests or calculated from numerical finite element computations (Thibert et al., 2008). As explained in that paper, we use the analytical Euler-Bernoulli beam model in good agreement with the 2 other possible calculations of the FRF. An additional point mass (190 kg) to the model is used to simulate the plate. This one was located at L_p=1.50 m from the clamped end during the avalanche released on the 15 February 2007.

Figure 2: Instrumented structure set up in path n°2. The 1 m^2 plate can be moved along the beam to be located exactly at the surface of the snow-cover.

3. RESULTS: AVALANCHE IMPACT PRESSURE RECONSTRUCTION

As detailed in (Thibert et al. 2008), snow and meteorological conditions on 15 February 2007 allowed artificial release of a quite large avalanche above the structure. We have used the data reported in that paper to develop here an error examination of the inverse analysis data process. The reconstructed load of this avalanche is obtained from the solution of the inverse problem given by the regularized deconvolution formula:

$$\hat{f}_\delta(\omega) = \frac{\hat{\varepsilon}_\delta(\omega)\cdot\hat{\phi}(\omega)}{\hat{h}(\omega)} \qquad (2)$$

where the symbol " ^ "denotes Fourier transform functions of the circular frequency variable ω.

Given that the FRFs can have very small amplitudes and that the measured signal ε_δ is polluted by the measurement noise, the direct deconvolution of Eq. (2) without regularization leads to instability of the inverse problem (Tikhonov and Arsenin 1977). The solution is therefore to find the optimal level of regularization between stability and accuracy. This optimal level is achieved using the Morozov discrepancy principle (Groetsch, 1993). The optimal value of regularization is here ω_c =25 Hz as obtained from the L-Curve (Groetsch, 1993) which reduces significantly the initial 0-1000 Hz bandwidth. Fig. 4 shows the L-Curve graph of the norm of the residual versus the solution. The reconstructed pressure from gage n° 1 is plotted in Fig. 5.

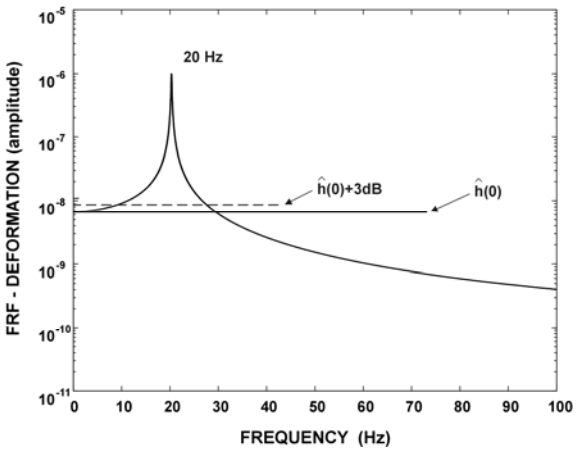

Figure 3: FRF as deduced from the Euler-Bernoulli direct model. Note that the value of 18.6 Hz was measured during hammer tests.

The maximum pressure is around 35 kPa for this avalanche. Despite the reduced bandwidth due to regularization, a dynamic analysis is still worthwhile in the frequency range covering the first Eigen mode of the structure (20 Hz). A constant frequency transfer function extrapolated from the static case would be:

$$\hat{h}(\omega) = \hat{h}(0) = \frac{L_p l}{2IE}, \qquad (3)$$

where E is the Young's modulus, and where other annotations are given in Fig. 6. The moment of inertia, I, equals 1.29x10^{-4} m^4 using data of Fig. 6. It results that $\hat{h}(0)$=6.50x10^{-9} N^{-1} using for structural S235 steel a Young's modulus of E=210 GPa. The static extrapolation to higher frequencies is not acceptable above 5 Hz as static and dynamic response functions differ from more than 3 dB (Fig.3).

4: DISCUSSION: ERROR ANALYSIS

Errors in the reconstructed pressure are determined considering various sources of uncertainties both in measurement and in the model. Calculations are done in two steps: first, static conditions are only considered and uncertainties in the deformation-to-pressure transfer function $\hat{h}(0)$ are quantified. Second, in order to take into account the frequency dependence of the FRF, an iteration of 500 inverse analyses is performed using a distribution of direct models resulting from Monte Carlo (MC) simulations.

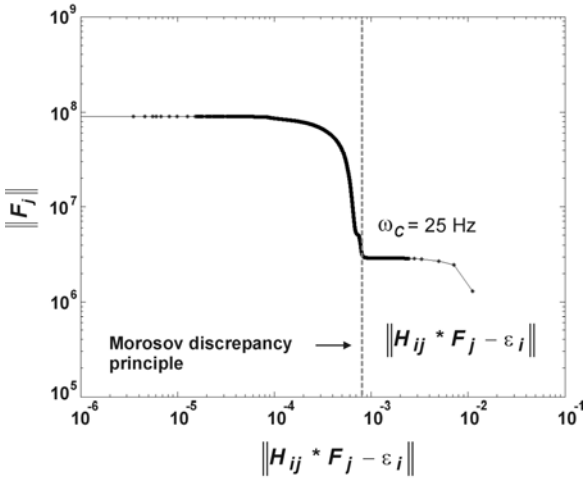

Figure 4: L-Curve determining the optimal cut-off frequency (25 Hz) of regularization according to the Morosov discrepancy principle.

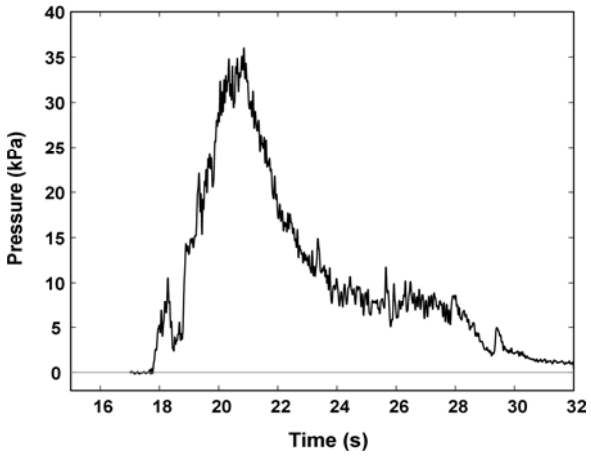

Figure 5: Reconstructed pressure for the avalanche released on 15 February 2007.

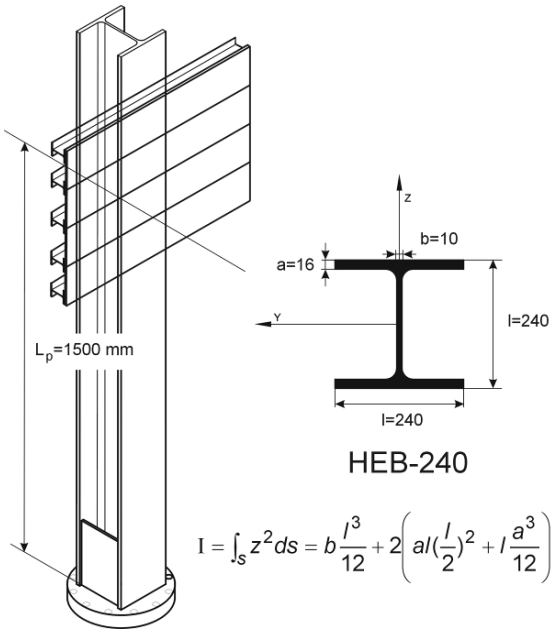

Figure 6: Geometry of the steel beam and the plate, and associated momentum of inertia, I, of the beam.

4.1 Static calculations

In the following, uncertainties are quantified by standard deviations and combined assuming they are uncorrelated. Under static conditions, the transfer function given by equation (3) links the pressure, *P*, to the measured deformation ε according to:

$$P = \frac{\varepsilon}{\hat{h}(0)} = \left(\frac{2\mathrm{I}E}{L_p l}\right)\varepsilon \,, \tag{4}$$

so that the error in the pressure (ISO, 1995) is:

$$\sigma_P^2 = \left(\frac{1}{\hat{h}(0)}\right)^2 \sigma_\varepsilon^2 + \left(\frac{\varepsilon}{\hat{h}(0)^2}\right)^2 \sigma_{\hat{h}(0)}^2 \,, \tag{5}$$

which highlights the contribution due to the measurement errors, σ_ε, and to the model error included in the FRF uncertainty $\sigma_{\hat{h}(0)}$ term. The first term in the right-end side of equation (5) can be calculated from equation (3) and from strain gage measurement noise, σ_ε, estimated in the signal before the avalanche reaches the structure ($4\text{x}10^{-6}$ m/m). The measurement error is therefore 0.62 kPa. Estimating the second term of equation (5) requires calculating the variance of $\hat{h}(0)$ from equation (3). This yields to (ISO, 1995):

$$\sigma_{\hat{h}(0)}^2 = \left(\frac{l}{2\mathrm{I}E}\right)^2 \sigma_{L_p}^2 + \left(\frac{L_p}{2\mathrm{I}E}\right)^2 \sigma_l^2 + \left(\frac{L_p l}{2\mathrm{I}}\right)^2 \frac{\sigma_E^2}{E^4} + \left(\frac{L_p l}{2E}\right)^2 \frac{\sigma_\mathrm{I}^2}{\mathrm{I}^4} \tag{6}$$

where the σ terms denote the uncertainties of the position of the plate on the beam (L_p), of the width of the beam (l), of the Young's modulus (E) and of the momentum of inertia (I).This last one is calculated from equation in Fig. 6 with typical production tolerances for dimension uncertainties ($\pm 2.5\ 10^{-4}$ m). This gives σ_I =1.79x10^{-6} m^4. The plate location uncertainty is σ_{L_p} =1 cm and the Young's modulus error is σ_E = 12 GPa. This results in an error on the static transfer function, $\sigma_{\hat{h}(0)}$, of 3.85x10^{-10} N^{-1} (a little less than 6% of $\hat{h}(0)$). Considering typical deformation measured during the avalanche (10^{-4} m/m) for a static load of 15 kPa, it results that the uncertainty in the pressure due to the model error is 0.91 kPa. The overall error given by equation (5) is therefore 1.10 kPa (7.3% of relative error) under static load conditions.

Table 1: Parameters used in the sensitivity analysis and their distributions. U and N letters denote the uniform and normal law of distribution (see text).

parameter	law	mean	U_{min}	U_{max}	σ	unit
boundary condition	U	100	95	105		%
plate position, L_p	U	1.47	1.46	1.48		m
Young's modulus, E	N	210			12	GPa
moment of inertia, I	N	129			1.8	10^{-6} m^4
beam length	U	3.5	3.49	3.51		m
additional plate mass	U	190	180	200		kg
steel density	U	7850	8046	7654		kg/m^3
beam section	N	100.8			1.34	10^{-4} m^2
damping coefficient	U	0.0033	0.0032	0.0034		
strain gages position	U	200	198	202		mm
beam width, *l*	U	240	239.75	240.75		mm
snow deposition	N	120			10	kg

4.2 Dynamic calculations

Under dynamic loading conditions, the FRF frequency dependence must be taken into account to quantify the model error. This is done first through a sensitivity analysis: the uncertainties related to different parameters and processes are identified and quantified in the deformation-to-pressure transfer function through probability distributions. This is summarized in Table 1 where twelve identified parameters are characterized by their distribution probability. Letter *U* denotes a uniform distribution between a minimum and a maximum (U_{min}, U_{max}) and letter $N(m, \sigma)$ denotes a normal distribution whose mean is *m* and variance σ. The real clamping condition of the beam is quantified (%) by its effect (shifting) on the 1^{rst} Eigen frequency corresponding to an ideal boundary condition.

The sensibility of the reconstructed pressure to these parameters is investigated to identify main parameters (Fig. 7). The influence is expressed in % of the total variance of the first Eigen frequency of the FRF. The overall variance is low with only 0.94 Hz. The most critical parameter is the degree of perfection of the clamping condition of the beam in its foundation which explains alone 63% of the total variance. The second one is the position of the plate on the beam (23%). Other parameters have much less influence on the FRF but are not negligible. The final step in the error analysis is to sample each parameter according to its distribution law (MC simulation). A population of 500 samples is extracted from the distribution laws of each parameter to calculate the corresponding transfer functions and to conduct inverse analyses to get a family of reconstructed pressure curves.

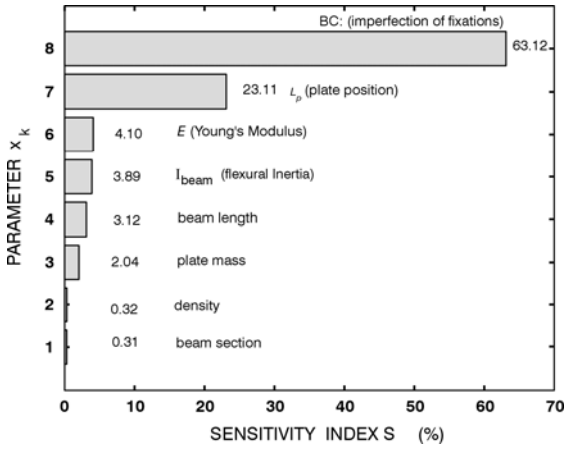

Figure 7: Influence of the 8 main parameters on the FRF in % of the total variance of the first Eigen frequency.

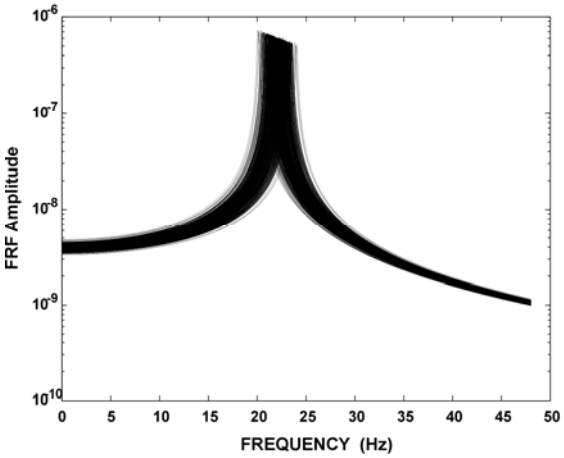

Figure 8: Distribution of FRFs as obtained from the samples of the MC simulation.

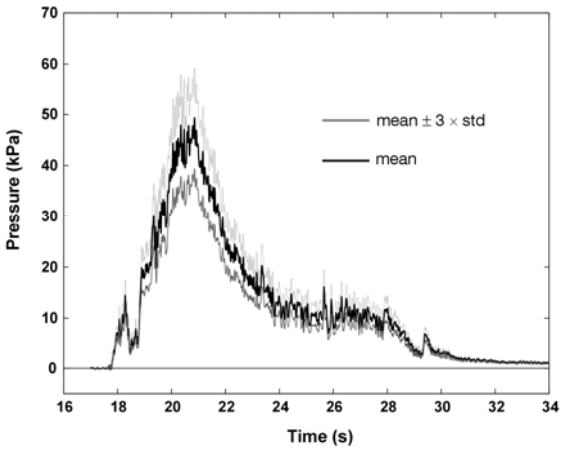

Figure 9: Mean pressure profile and pressure profiles at $\pm$ 3σ as estimated from MC simulations.

Fig. 8 shows the distribution of the 500 FRFs. The mean Eigen frequency is 20.98 Hz. FRFs have lower amplitudes than the FRF plotted in Fig. 3 because of the additional mass of 120 kg which is taken into account to simulated snow deposition on the plate (Thibert et al., 2008). Lower transfer function amplitudes result in higher reconstructed pressures compared to the initial pressure profile plotted in Figure 5. The model error calculated from MC simulation is typically 1.25 kPa over the pressure profile of Fig. 9. The relative error can be considered as roughly constant (6.4%) yielding to a maximum of 3 kPa at the pressure peak. This mean error is slightly greater than the model error calculated under static load conditions (5.9%). This is related to the FRF whose mean over the bandwidth (0-25 Hz) is higher than $\hat{h}(0)$.

The error of the model is combined to the measurement error to get the overall error as done under static load conditions. This is done assuming that the measurement error is not a function of the frequency over the bandwidth 0-25 Hz. Figure 10 confirms such a hypothesis as noise in the deformation signal before the avalanche reaches the structure has a spectrum which can be considered as not frequency dependent. Note that regularization cannot, however, completely eliminate the effect of measurement noise and the model error cannot be completely uncorrelated to the measurement errors. However, because this even effect is minimized by regularization, these both types of errors will be combined assuming they are uncorrelated.

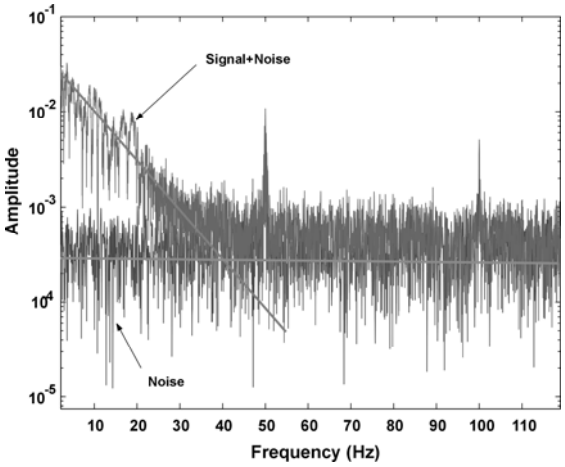

Figure 10: Frequency spectrum of deformations. The upper curve is the signal and noise during the avalanche. The lower curve is the noise without physical signal (before the avalanche) which does not depend on the frequency.

The measurement contribution to the overall error will be therefore considered as an additional term of 0.62 kPa as estimated in the static condition calculations. The overall error is therefore given as a function of time by:

$$\sigma_P^2(t) = \left(\frac{\sigma_\varepsilon}{\hat{h}(0)}\right)^2 + (0.064 x P(t))^2 = \\ = 0.378 + 0.004096 x [P(t)]^2 \quad (\text{kPa})^2, \qquad (7)$$

where *P(t)* is the pressure obtained from inverse analysis expressed in kPa.

4: CONCLUSION

The purpose of this paper was to provide an error analysis in the estimation from inverse analysis of the impact pressure of an avalanche that was reported in our previous study (Thibert et al. 2008). The error can be decomposed in 2 contributions. The first is related to strain measurement errors due to noise in the gage signals. It can be estimated under static loading conditions of the instrumented structure and is about 0.6 kP. The second contribution is related to uncertainties in the model used in the inverse analysis. A sensitivity analysis of the parameters included in the model shows that the main sources of error are the clamping conditions of the structure in its foundation and the position along the beam of the 1 m^2 plate

where the avalanche pressure of is applied. A Monte Carlo simulation shows that the relative error of the model is constant and about 6.4% of the reconstructed pressure from the inverse analysis. The overall (measurement + model) error for our experimental set-up and associated data process is therefore typically ±3.6 kPa for a 50 kPa pressure avalanche.

5. ACKNOWLEDGEMENTS

This work was supported by the Pôle Grenoblois Risques Naturels (Conseil général de l'Isère), and the ANR-OPALE project.

6. REFERENCES

Abe, O., Nakamura, H., Sato, A., Numano, N., Nakamura, T., 1992. Snow block impact pressures against on a wall, a post, and disks. Proceed. of the Japan-US workshop on snow avalanche, landslide, debris flow prediction and control, pp. 151-159.

Berthet-Rambaud P., Baroudi D., A. Limam, E. Thibert, Taillandier J.-M., 2008. Characterization of avalanche loading on impacted structures: a new approach based on inverses analysis. J. Glaciology, 54(185), 324-332.

Gerardin, M. and Rixen, D., 1993. Théorie des vibrations: application à la dynamique des structures. Masson, Paris.

Groetsch, C.W., 1993. Inverse problems in the mathematical sciences. Vieweg, Wiesbaden (Germany).

ISO guide 98, eds. 1995. Guide to the expression of uncertainty in measurement (GUM). ISO, Geneva (Switzerland)

Issler, D., 1999. European Avalanche test sites. Overview and analysis in view of coordinated experiments. Issler, D. (Ed.)., Eidg. Inst. Schnee und Lawinenforsch, Mitt. 59.

Kawada, K., Nishimura, K., Maeno, N., 1989. Experimental studies on a powder snow avalanche. Ann. of Glaciol. 13: 129-134

Lang, T. and Brown, R.L., 1980. Snow avalanche impact on structures. J. Glaciol., 25 (93): 445-455.

McClung, D.M. and Schaerer, P.A., 1985. Characteristics of flowing snow and avalanche impact pressures. Ann. Glaciol., 6: 9-14.

Meirovitch, L., 1986. Elements of vibration analysis. McGraw-Hill, New York, 2nd edition.

Nishimura, K. Narita, H., Maeno, M., Kawada, K., 1989. The internal structure of powder snow avalanches. Ann. of Glaciol. 13, 207-210

Norem, H., Kvisterøy, T. and Evensen, B.D., 1985. Measurement of avalanche speed and forces: instrumentation and preliminary results of the Ryggfonn project. Ann. Glaciol., 6: 19-22.

Schaerer, P.A., and Salway A.A., 1980. Seismic and impact-pressure monitoring of flowing avalanches. J. Glaciol., 26 (94): 179-187.

Schaer, M. and Issler, D., 2001, Particle densities, velocities and size distributions in large avalanches from impact-sensor measurements, Ann. Glaciol., 32: 321-327.

Sovilla, B., Schaer, M., Kern, M., Bartelt, P., 2008. Impact Pressures and flow regimes in dense snow avalanches observed at the Vallée de la Sionne test site. J. Geophys. Res. 113(1) art. no. F01010

Thibert, E., D. Baroudi, A. Limam, P. Berthet-Rambaud, 2008. Avalanche impact pressure on an instrumented structure. Cold Regions Science and Technology. doi: 10.1016/j. coldregions .2008.01.005

Tikhonov, A.N. and Arsenin, V.Y, 1977. Solutions of ill-posed problems. Wiley, Chichester (England).